THE JOURNAL OF PHYSICAL CHEMISTRY C

C: Physical Processes in Nanomaterials and Nanostructures

Graphene Grown on Ni Foam: Molecular Sensing, GERS, and Galvanic Exchange for SERS Applications.

Maria Mercedes Messina, Andrea Lorena Picone, Paula Cecilia dos Santos Claro, Remigio Ruiz, Fabio D. Saccone, Rosana Mariel Romano, and Francisco Javier Ibañez

J. Phys. Chem. C, **Just Accepted Manuscript** • DOI: 10.1021/acs.jpcc.7b12021 • Publication Date (Web): 02 Apr 2018

ACS Publications

is published by the American Chemical Society. 1155 Sixteenth Street N.W., Washington, DC 20036

Graphene Grown on Ni Foam: Molecular Sensing, GERS, and Galvanic Exchange for SERS Applications.

M. Mercedes Messina,[†,⊥] A. Lorena Picone,[‡] P. Cecilia dos Santos Claro,[⊥] Remigio Ruiz,[£] Fabio D. Saccone,[⊥,#] Rosana M. Romano,[‡] and Francisco J. Ibañez[†]*

[⊥] Gerencia de Ambiente, Biotecnología y Energías Renovables. YPF Tecnología S. A., Av. Del Petróleo S/N (e/129 y 143), (1923) Berisso, Buenos Aires, Argentina.

[#] Departamento de Física, Facultad de Ingeniería, Universidad de Buenos Aires, Av. Paseo Colón 850, (1963) CABA, Argentina.

[‡] CEQUINOR (UNLP, CCT-CONICET La Plata). Departamento de Química, Facultad de Ciencias Exactas, Universidad Nacional de La Plata. Blvd. 120 N° 1465, CC 962, La Plata (CP 1900), Argentina.

[£] Gerencia de Geociencias. YPF Tecnología S. A., Av. Del Petróleo S/N (e/129 y 143), (1923) Berisso, Buenos Aires, Argentina.

[†] Instituto de Investigaciones Fisicoquímicas, Teóricas y Aplicadas (INIFTA). Universidad Nacional de La Plata - CONICET. Sucursal 4 Casilla de Correo 16 (1900) La Plata, Argentina.

Author to whom correspondence should be addressed: fjiban@inifta.unlp.edu.ar

ABSTRACT.

The growing of graphene on irregular 3D Ni structure demonstrates to be an interesting platform for, molecular sensing, GERS, and SERS applications after galvanic exchange of Ag^+ ions. Raman, SEM (EDS), optical images, and diffuse reflectance exhibit that graphene grows in multilayer (MLG) fashion with different stacking configurations. Statistics performed employing Raman show that as-grown graphene can be classified in two main stacking configurations: AB (or Bernal stacking) and rotated graphene which are separated by a 2D full-width half maximum (fwhm) threshold of ~30 cm^{-1}. Rotated stacking senses low concentrations of methylene blue (MB) at 10^{-6} M concentration, whereas AB-stacking seems to be much less sensitive upon molecular adsorption. Galvanic exchange of Ag leads to agglomerates preferentially formed on top graphene wrinkles which ultimately became target-spots for performing SERS. Our experiments demonstrate that as-grown graphene, comprised of different stacking configurations, can be used as a molecular sensor and detect nanomolar concentrations of MB and thiram (by SERS applications), after galvanic exchange with Ag.

INTRODUCTION

Three dimensional (3D) carbon structures brings about new fundamental studies and applications that involve separation of contaminants in oil,[1] supercapacitors,[2] Li-ion batteries,[3] and less explored the detection of low concentrations of analytes via surface-enhanced Raman Scattering (SERS) technique.[4] The chemical vapor deposition (CVD) method employed for Ni foam is quite intriguing since it consists on growing a 2D

nanocarbon on a bulky 3D scaffold which is fully comprised of borders, pits, and curved areas. Raman spectroscopy is a powerful technique that has become a finger print for characterizing 2D nanomaterials[5,6] as well as being exploited, in combination with graphene, toward surface techniques such as graphene-enhanced Raman scattering (GERS)[7] and SERS.[8] The use of metallic nanoparticles (NPs) for SERS applications has proven to be an excellent approach for the detection of extremely low concentrations of analytes.[9,10,11] Our group recently combined the attributes of metallic NPs with graphene toward SERS[12] and tip-enhanced Raman scattering (TERS)[13] applications because the former nanomaterial provided plasmons (and hot-spots) while the later quenched most of the fluorescence[14] and photoluminescence[15] evolved by the analyte and NPs, respectively. All those experiments were performed on CVD grown graphene on Cu later transferred to the desired substrate. CVD graphene on Ni catalyst is different because the solubility of carbon atoms in Ni is 50 times greater than Cu.[16,17] That ensures full diffusion and precipitation of carbon along the entire catalytic surface[18,19] and brings about new challenges regarding its characterization. For example, the main Raman bands of graphene (G and 2D) sometimes have not been observed[20] after CVD graphene on Ni which at first glance, may imply that graphene did not grow under the area of study. Another possibility is that the strong hybridization between π-orbitals in monolayer graphene and d-electrons from Ni may suppress the Raman signals.[21] Another example is that graphene grows in a multilayer stacking and therefore it is possible to find different stacking configurations which may include rotated graphene and AB (or Bernal stacking).[22,23]

Rotated stacking (also named “misorientated”) graphene is characterized by intense and narrow 2D Raman band, and sometimes an intense G band depending on the type of

rotation (i.e., whether the angle of rotation is close to a critical angle).[24] Rotated configuration can be easily confused with SLG likely because the Raman band profiles (i.e., 2D line width and intensity ratio 2D to G band) are very similar. Some of the physical chemistry properties in rotated graphene have shown to be also similar to SLG graphene as demonstrated by theoretical predictions[24] and recent experiments[25,26] whereas, AB stacking behaves much more like graphite.[27] As an example, Weis *et al.* employed ^{13}C and ^{12}C isotopes to unambiguously distinguish between the two layers in a bilayer graphene configuration upon incorporation of fluorine ions. They compared monolayer vs. bilayer graphene and rotated vs. AB-stacking at the bilayer configuration. It was demonstrated that sensitivity (measured by a shift of the G band) decreases as the number of layer increases and stacking configuration changes upon chemical doping in the following order: monolayer graphene > bilayer (rotated) > bilayer (AB-stacking).[25] Recent experiments performed by Jarrillo-Herrero and co-workers have revealed an unprecedented behavior in rotated bilayer graphene. They reported on the existence of a magic angle of rotation between two twisted graphene layers which allows superconductivity.[28] These experiments confirmed that not only the number of layers play a crucial role but also, the type of stacking (and angle of rotation between layers) toward the ability of graphene properties to be further tailored either by decoration of metal NPs[29] or adsorption of molecules.[30,31,32] There are few different methods for obtaining a heterojunction composed of graphene and metallic NPs. For instance, Kamat and co-workers employed electrons generated by UV illumination on TiO_2 NPs sitting on top of graphene oxide (GO_x) for simultaneously reducing Ag^+ ions and GO_x.[33] Our group recently demonstrated the spontaneous adsorption of organic-coated Au NPs on graphene[12] as well as the use of the same NPs for transferring graphene without the use of polymers.[13] Other methods employ galvanic exchange of

metallic ions however, this procedure has been performed directly on bare Ni foams[34,35] and metal dendritic structures[36,37] without the presence of graphene. This may be a result of knowing that graphene grows in multilayer stack and may cover the entire Ni surface. These two factors may have prevented ion-exchange between metallic Ni and ions in solution.[38]

In this work, we show that multilayer graphene grows on irregular 3D structure which is later exchanged with Ag ions. Growing graphene on a Ni structure is beneficial in many ways because ensures full graphene coverage, provides sharp spots due to the irregular surface, leads to two main stacking configurations with different properties that can be exploited toward molecular sensing/doping, GERS, and permits the formation of Ag agglomerates on top graphene which is ideal for SERS applications. We demonstrate that graphene can be classified into two main stacking configurations which include rotated and AB-stacking. Rotated graphene is particularly sensitive to low concentrations (10^{-6} M) of MB as demonstrated by changes on its Raman band profiles while AB-stacking seems to be insensitive. Galvanic displacement may result impossible to achieve without the use of any external source of energy[39] considering that graphene grows all over the surface and that ions may have to trespass several graphene layers. Surprisingly, our experiments show that Ag^{+} ions not only exchanged on top of graphene but also preferentially on wrinkles formed during the CVD synthesis. Ag NPs deposits were later used as target-spots for detection of small concentrations of thiram and MB. Thiram is a fungicide widely used to prevent crop damage however, people may be exposed to residues through the diet therefore it is highly required to be detected in low concentrations.[40]

EXPERIMENTAL METHODS.

Chemicals. Sodium borohydride ($NaBH_4$, 99%), tetraoctylammonium bromide ($C_{32}H_{68}BrN$, 99%), toluene (C_7H_8, 99.9%), ethanol (C_2H_6O, 200 proof), acetone (C_3H_6O, 99.9%), silver nitrate ($AgNO_3$, 99.9%), tetrachloroauric acid ($HAuCl_4$), were purchased from Aldrich Chemical Co. Nickel foam (thickness 1.6mm, porosity 87%). Thiram (dimethylcarbamothioylsulfanyl N,N-dimethylcarbamodithioate, $C_6H_{12}N_2S_4$, 98%) and 7-(dimethylamino)phenothiazin-3-ylidene]-dimethylazanium; chloride ($C_{16}H_{18}ClN_3S$) known as Methylene Blue (MB) were purchased from Merk. H_2 (99.999%) and CH_4 (99.999%) gases were purchased from Linde Argentina. Milli-Q water (17.8 MΩ·cm) was employed for all aqueous solutions.

Synthesis of 3D Graphene on Ni Foam. Graphene was grown by chemical vapor deposition (CVD) method on Ni foam.[41] Before grown, the Ni foam (Nif) was sonicated three times 20 min in acetone and placed at the center of a quartz tube furnace pumped to 8.0×10^{-5} Torr. After reaching a steady pressure, 75 mL/min of H_2 was constantly passed through the tube during the entire synthesis. The sample was annealed at 950 °C for 30 min, and then 35 mL/min of CH_4 was flowed for 5 min for graphene synthesis. After the exposure to CH_4 the substrate was cooled down to room temperature (cooling rate: 16 °C/min).

Synthesis of Tetraoctylammonium bromide Coated Au Nanoparticles (TOABr-Au NPs). The TOABr-coated Au NPs were synthesized according to the two-phase Brust−Schiffrin reaction but without the addition of organic thiols.[42] Details of the synthesis were reported somewhere else.[43]

Heterojunction Formation. Galvanic exchange of Ag ions on as-grown graphene (Ag exchanged). The as-grown graphene was immersed in an aqueous solution of 0.1 M $AgNO_3$ during 1.0, 2.5, and 5.0 minutes in order to deposit Ag nanoparticles on the surface following a galvanic displacement reaction. The substrate was soaked two times in Milli-Q water and then dried at 60ºC for 1h prior to Raman experiments. **Adsorption of Surfactant Coated-Au NPs (Au adsorbed).** The as-grown graphene was immersed in a concentrated toluene solution of TOABr-Au NPs for 3 hours. Au NPs spontaneously adsorbed to the 3D graphene structure due to hydrophobic interactions between graphene and the organic ligands.[12] The sample was then soaked in absolute ethanol, dried, and heated at 200 °C for 1 hour in a tube furnace in order to remove the organic material. Finally, the sample was soaked again in ethanol and dried with N_2 gas.

Characterization. Raman spectra were acquired in a Jasco NRS-4100 micro-spectrometer, equipped with a 900 g/mm grating and an edge filter. The excitation beam was provided by a green laser at 532.34 nm with 20 mW of power. Raman signal was collected using a 20× objective (0.4 NA-Olympus) and 100% laser intensity resulting in ~6 mW at the sample. A rectangular slit (200 x 8000 μm) was used and the acquisition time was 5 s for every 5 averaged spectra. A Si standard was used for wavenumber calibration of Raman spectrometer. Scanning electron microscopy (SEM) images and energy-dispersive X-ray spectrum (EDS) were acquired on a FEI QUANTA 200 with accelerating voltage between 20-25 keV. Optical images were captured by an Olympus BX51 microscope. Diffuse reflectance measurements were carried out using a Shimadzu UV 2600/2700 spectrophotometer equipped with an integrating sphere. The equipment was calibrated with

a $BaSO_4$ standard and all measurements were collected using the standard as background. The diffuse reflection spectra were measured between 220-800 nm.

Raman active platforms. MB and thiram powders were dissolved in Milli-Q water and absolute ethanol, respectively, to form stock solutions. Then, the stock solutions were further diluted to prepare different concentrations from 10^{-5} to 10^{-10} M. All the substrates prepared in this work were incubated in MB or thiram solutions at the above concentrations. Each sample was immersed in 1 ml of solution for 30 min in order to provide enough time for adsorption of analyte molecules. The samples incubated in MB solutions were then dried in an oven at 60 °C for 30 minutes before SERS measurements. The samples incubated in thiram solutions were dried in air for few minutes before the SERS measurements. To estimate the magnitude of enhancement, Raman signal from each solid analyte was measured using a capillary tube. These measurements were carried out with the same parameters selected for SERS platforms.

SERS experiments. Raman measurements performed to detect MB and thiram molecules were carried out employing the same parameters but with a circular slit (d-100μm) and 50% laser intensity (resulting in ~3 mW at the sample) in order to avoid laser-induced heating. In addition to the green laser (Jasco NRS-4100 micro-spectrometer), a dispersive Horiba-Jobin Yvon T64000 confocal microscope Raman spectrometer, with a CCD detector, was employed in subtractive mode to carry out the measurements using a red laser at 647.1 nm. The samples were excited with a red light from a Coherent Kr multiline laser with 100 mW of output power. Raman signal was collected using a 50x objective (0.75 NA). The acquisition time was 20 s for every 4-averaged spectrum.

RESULTS AND DISCUSSION.

Characterization of Graphene Grown on Ni foam. Figure 1A shows representative micro-Raman spectra of five different spots recorded from the same sample after CVD grown graphene. The Figure also exhibits optical and SEM images before and after as-grown graphene. Both, optical and SEM images show clear and dark areas indicating non-uniform growth on the Ni surface. There are few particular aspects that need to be addressed from the spectra in Figure 1A. First, the spectrum indicated as "as-grown G" corresponds to CVD graphene sample although; it does not exhibit any particular Raman band of graphene whatsoever. Vacant areas may be consistent with areas whereby graphene did not grow as it usually occurs during CVD performed on Cu[44] or other metals.[20,45] The potential absence of graphene may be also consistent with bright areas observed in optical and SEM images. We performed Raman and EDS on multiple areas of the sample indicated by green circles and arrows in Figure 1 C and D, respectively and systematically found the presence of carbon including bright spots as the one labeled "2" which corresponds to 12 % carbon content. This clearly suggests that graphene grows all over the Ni surface but in different carbon amounts indicating more or less number of graphene layers. Our results are consistent with the literature that has shown similar spectra profiles[20] for bright areas on CVD grown graphene associated with a strong hybridization between d-bands from Ni and π-electrons in graphene.[16,21] This suggests that graphene may have grown in single or few layers stacking although their characteristic Raman bands could not be seen because of the aforementioned strong affinity with the metal catalyst. Moreover, based on the high solubility of carbon in Ni during the CVD

method, it is more likely to find MLG than SLG. Nevertheless, the absence of Raman bands has been rarely observed and therefore it is not further discussed here.

Second, the other spectra in Figure 1A show a full umbrella of possibilities ranging from "graphitic-like" to "monolayer-like" graphene if we move from the bottom to the top spectra. Monolayer graphene is known by a sharp 2D band whose intensity exceeds 3x or more that of the G band. Here again, graphitic-like spectra were rarely seen during the experiments and therefore not included. The spectrum that exhibits an intensity ratio (I_{2D}/I_G) less than 2, broad 2D band (~45cm^{-1}), and 2D blue shifted wavenumber is referred to AB-stacking which is a common configuration in MLG and graphite. The other two spectra were named rotated-H (high) and -L (low) because they exhibit high and low I_{2D}/I_G intensities ratios, respectively. They also exhibit much sharper 2D fwhm relative to AB stacking. The spectra referred as "rotated-H" with intensity ratio (I_{2D}/I_G) equal or greater than 3 can be easily confused with SLG however, it corresponds to multilayer where each layer is rotated at different angles with respect to the other.[46,47] It has been demonstrated that this type of spectrum corresponds to rotation angles larger than a critical angle.[24] In addition to the striking intensity of the 2D band, the difference between SLG and rotated-H is determined by the appearance of "in-plane" and "rotation modes" which will be discussed in the following section. The reason why the electronic 2D band is so intense in rotated MLG, relative to AB-stacking, can be explained on the bases of weak interlayer interactions.[24] This configuration is particularly interesting since the weak interaction between layers allows high charge carrier mobility as well as interesting optical properties such as absorption bands in the visible range.[48,49,50]

Rotated versus AB-stacking. Figure 2 exhibits a plot of intensity ratio of the 2D to G bands (I_{2D}/I_G) vs. fwhm of the 2D band taken from 23 different areas of the as-grown graphene. On the side of Figure 2 there are representative Raman spectra for each type of staking configuration. Full spectra are shown in Figure S1 and S2. There are few particular aspects of as-grown graphene that distinguish both configurations. First, there is a 2D fwhm threshold around ~30 cm^{-1} that circumscribes the majority of data points in two major populations. Above that threshold there is solely AB-stacking whereas below coexists two types of rotated graphene (vide supra) exhibiting a full range of 2D : G intensities ratios ranging from high ~(9 : 1) to low ~(1 : 1) ratios. There is another minor region in the plot corresponding to a combination of both stackings labeled "mix". This region falls within the threshold for both main configurations and has been less frequently detected. Second, rotated and AB-stacking are also distinguishable by the appearance of "in-plane" and "out of plane" bands[51,52] observed at ~1890 (LO + TA mode) and ~2034 cm^{-1} (TO + LA, LO + LA modes) for the former and at 1753 cm^{-1}(LO + ZO′ mode) for the later, as shown next to Figure 2. Among the rotated configurations, when the angle of rotation is close to the critical twisting angle, two new bands appear at 1488 and 1448 cm^{-1} (known as rotational modes, R)[23] (see small spectra next to Figure 2), and the G band dramatically increases occasionally matching up the intensity of the 2D band (Figure 1A). Furthermore, it can be distinguished a breathing mode (ZO′)[53] located at 126 cm^{-1} whose band intensity increases along with the G band as shown in Figure 1A. Finally, we systematically noticed the presence of a D band regardless the type of stacking which indicates the presence of defects on as-grown graphene. It is reasonable to think about defects since the Ni scaffold is a tortuous 3D structure that offers many surface imperfections to CVD graphene. We attempted to associate those two stacking

configurations to any particular topography on the surface that may reassemble curved areas on graphene[54] or borders in graphitic foams[55] however, we found no correlation so far.

Molecular Sensing. Since one may encounter different stacking configurations (with different physical properties) within few microns on the same sample we tested the ability of as-grown graphene upon molecular sensing of MB. Figure 3 exhibits a dispersion plot of intensity ratio (I_{2D}/I_G) vs. fwhm of the 2D band taken from 5 different spots before and after the addition of MB as indicated by the optical image in the inset. We chose five topographically different areas (i.e., inset shows Raman spots 2 and 4 on a pit and border) in order to see if there is any correlation between structure and stacking. It should be mentioned that micro-Raman experiments were performed on exactly the same spots before and after addition of 1.0×10^{-6} M MB, as indicated. It should be also noted, that all the Raman data in Table 1 corresponds to rotated-H graphene sample despite the strikingly different topography. After incorporation of MB, the 2D to G intensity declines while the 2D band slightly shifts and widens. The drop-in intensity ratio from ~3.5 to ~2.0 was generally caused by a drop of the 2D band and in some minor cases accompanied by an increase of the G band intensity after adsorption of MB. Table 1 shows intensity ratio, 2D fwhm and Raman shift, and average Raman shift and intensity ratio before and after addition of MB measured from those five different spots shown in the inset. There is a systematic red-shift of the 2D band after the incorporation of MB indicating electron transfer from these planar molecules to the graphene film. This is remarkable since small analyte concentrations induce large changes in Raman bands at this particular stacking configuration. By the contrary, a control experiment performed on 3 different areas

corresponding to AB-stacking exhibited poor or no changes after incorporation of the same concentration of MB. This indicates that rotated graphene is the most sensitive configuration between these two main types of stackings. Figure S3 shows representative spectra for rotated and AB-stacking configurations before and after MB. It should be noticed from Figure S3 that MB peak at ~1624 cm^{-1} is observable for both cases indicating that meanwhile both stacking configurations are capable of GERS, regardless the type of stacking, only rotated graphene senses low concentration of MB. The possibility of returning to exactly the same micro-Raman spot allows choosing the most sensitive stacking prior sensing. We will further explore this configuration upon sensing lower analyte concentrations.

Galvanic Exchange of Ag ions and Metal Doping. Figure 4 shows selected Raman spectrum for a rotated-H configuration, optical and SEM images before and after Ag galvanic displacement; respectively. Green arrows, in the SEM images, point out the presence of wrinkles in graphene before and after electroless deposition of Ag NPs. It is clear from the spectrum that Ag NPs caused ~4-fold increase of most of the graphene bands including those in-plane modes characteristic of rotated graphene as shown in Figure 4A. Once the as-grown graphene is immersed in $AgNO_3$ solution for 5 min, galvanic displacement occurs leading to the formation of large Ag NPs and some agglomerates on specific sites of graphene as noticed by the SEM image. EDS performed on top of those Ag agglomerates exhibited the presence of carbon indicating that they were effectively formed on top of graphene. This further suggests that Ag^+ ions exchange on top of carbon layers and more preferentially on defect areas such as wrinkles where nucleation and growth of Ag seems to occur. Accordingly, in the presence of aqueous solution of Ag

ions, Ni should oxidize to Ni^{2+} and then graphene may act as electron shuttle favoring reduction of Ag ions on remote areas of the film.[56] Since the platform mainly consists on MLG stacked in different configurations, electrons should make their way toward the interface graphene-Ag ions solution to finally accomplish galvanic displacement.[57]

Our group previously constructed heterojunctions (metal-graphene) by decorating graphene with surfactant-coated metallic NPs (usually Au) but it was not very effective because the heterojunction needed further treatments for removing the organic coating.[12] Galvanic exchange is a promising approach since does not involve organic ligands or polymers which may prevent, for instance, the detection of low analyte concentrations by SERS. Figure 5A compares characteristic Raman bands of as-grown graphene with Ag galvanic exchange and adsorbed Au NPs. After galvanic exchange, the spectrum exhibits broadening of the G band along with a small shoulder assigned to D' (located at 1620 cm^{-1}), exaltation of D band at 1350 cm^{-1}, and the appearance of D + G band. These spectral features have been previously reported for Ag nanoparticles deposition on single and few layer graphene.[58,59] On the other hand, adsorption of Au NPs seems to have a minor effect on graphene likely due to the presence of organic ligands around the NPs. Raman bands in graphene can be modified via transferring electrons or holes from metallic NPs,[29] therefore Figure 5B compares fwhm vs. Raman shift from the 2D band measured for the three platforms involved in this study. After Ag exchange, there is a broadening of the G band accompanied by a noticeable down-shift (by ~4 cm^{-1}, see Table 2) of the 2D band which indicates n-doping of graphene associated with the difference in work function.[60] These differences in Raman spectra for metal NPs on graphene suggest that the deposition method may play an important role. Also, the topography of adsorbed Au NPs film (~ 5 nm diam.)

is different to Ag exchange because the former film exhibited uniform distribution along the entire platform (see SEM images in Figure S4). We also noticed that the presence of graphene led to an increase in the absorbance in the visible range which is slightly modified by Ag and Au NPs deposits (See Figure S5). In conclusion, galvanic exchange method seems to be a more suitable approach since the interaction metal-graphene seems to be stronger, there are no organic ligands around the NPs, and the formation of agglomerates may be beneficial for further applications in SERS.

SERS activity. SERS activity was investigated using MB and thiram adsorbed on the as-grown graphene exchanged with Ag^+ ions (referred to exchanged Ag). Figure S6 compares the SERS spectra of 1.7 x 10^{-5} M MB adsorbed on all the different platforms employed in this work which includes Ni foam, as-grown graphene, and as-treated graphene (exchanged Ag and adsorbed Au). Figure S6 shows that higher signal intensities arise from the Ag exchanged platform. For example, the band located at 1626 cm^{-1}, whose intensity is almost three times higher for Ag than Au, demonstrates the importance of the metal composition. Based on these results, we explored into SERS of MB employing the aforementioned platform. Figure 6A shows Raman spectra of the platform measured at various concentrations of MB ranging from 10^{-5} to 10^{-9} M, compared with Raman signal from the solid analyte, using a green laser at 532 nm. To investigate the sensitivity of the platform, the peaks located at 1396 and 1626 cm^{-1} were evaluated. Figure 6B shows a plot of SERS intensity vs. MB concentration. Plotting 1/SERS intensity vs. 1/[MB] for the band at 1626 cm^{-1} exhibited (data not shown) a well fit to the Langmuir isotherm as indicated by a regression coefficient and an equilibrium constant of 0.989 and 2.5 x 10^7, respectively.[61] Figure 6C exhibits SERS intensity vs. logarithm of MB concentration observed for both

peaks mentioned previously. Considering that Ag coverage and agglomeration may influence SERS performance, we exposed as-grown graphene to different exchange times. Figure S7 exhibits the optimal enhancement ability of the platform after 1, 3, and 5 min of Ag galvanic exchanged on as-grown graphene. The optimal SERS performances were achieved with the longer exchange time and placing the laser on top of Ag agglomerates as shown in Figure S8. The Raman spectrum in Figure 6A shows that all bands located at 446, 1396 and 1626 cm^{-1} can be observed using this optimal time. The enhancement factor (EF) of the platform was calculated according to the following formula:[34,62]

$$EF = \frac{I_{surf}/N_{surf}}{I_{bulk}/N_{bulk}} \quad (1)$$

where I_{surf} and I_{bulk} are the peak intensities at 1396 cm^{-1} for 10^{-9} M MB on the platform (SERS) and from MB solid powder (conventional Raman), respectively. N_{surf} and N_{bulk} represent the number of molecules located in the region of the laser beam in the SERS and conventional Raman spectroscopy, respectively. The conventional Raman and SERS spectra were measured under the same parameters of acquisition time, slit, excitation wavelength, and laser power. N_{surf} can be calculated following this equation:

$$N_{surf} = \frac{A\, C_{surf} V\, N_a}{A'} \quad (2)$$

where A is the area of laser spot (2.01 μm^2), C_{surf} is the concentration of the MB solution ($1.7x10^{-9}$M), V is the volume of MB solution in which was immersed the platform (1 mL), Na is the Avogadro constant, and A' is the area of the platform ($0.25cm^2$).

N_{bulk} can be calculated from the equation:

$$N_{bulk} = AhC_{bulk}N_a \qquad (3)$$

where C_{bulk} is calculated from the molar mass and density of MB solid analyte ($C_{bulk}= \rho/M$), and h is the effective height calculated experimentally (11 μm). From the experimental data, the EF ratio is estimated to be 9.3×10^4 for $1.7x10^{-9}$ M MB adsorbed on the active platform. We occasionally observed the band located at 1626 cm^{-1} for concentrations of MB as low as 1.7×10^{-10} M (data not shown).

Figure 7A and 7B compare Raman spectra of the platform employing green and red laser, respectively at three different concentrations of thiram (10^{-5}, 10^{-7}, and 10^{-9} M) with Raman signal aroused from the solid analyte. It can be observed that in both cases SERS intensity is proportional to thiram concentration. This dependence is clearly observed in the plot 7C which shows SERS intensity versus the logarithm of thiram concentration at 1386 cm^{-1}. From the experimental data and considering a green laser, we estimate an enhancement EF ratio of 1.5×10^5 for 10^{-9} M thiram adsorbed on the SERS platform. To

evaluate the role of graphene in SERS performance, we compared Raman spectra of Ag galvanic exchange performed on Ni foam with and without graphene (Fig. S9-A) and 1 x 10^{-9} MB adsorbed on both aforementioned platforms (Fig. S9-B). The Raman spectra without graphene exhibited mounted background in a frequency range between 1100 and 1700 cm^{-1} attributed to photocarbonization caused by the laser on traces of carbon material previously deposited from the ambient air.[63] The platform containing graphene, on the other hand, shows no background along with a cleaner signal that is further noticeable when dye molecules are incorporated. Interestingly, Figure S9-B shows that the platform with graphene allows detecting concentrations of analyte as low as 10^{-9} M. These results further demonstrate that this platform is suitable to be used as an active substrate for detection of trace level molecules.

CONCLUSIONS. In conclusion, it has been demonstrated that graphene on Ni foam grows into multilayer stacking that can be classified into two major configurations. We found a threshold of ~30 cm^{-1} corresponding to the 2D line width which divided rotated graphene from AB-stacking configuration. Rotated graphene is characterized by relatively intense G and 2D bands and sharp 2D line (sometimes as sharp as 24 cm^{-1}) which were affected by the absorption of small concentrations of MB (1.0 x 10^{-6} M) as demonstrated by Raman experiments performed on the same spots before and after addition of the analyte. These findings may position as-grown graphene as a good candidate for molecular sensing which occasionally may compete with GERS and SERS applications. The galvanic exchange of Ag on as-grown graphene brought about interesting aspects. Ag^{+} ions exchanged preferentially on graphene wrinkles as demonstrated by Raman, SEM and EDS. This indicated that electrons arising from Ni^{2+} find their own way through several layers to

ultimately reach out the interface graphene-Ag^+ solution in order to reduce Ag^+ to metallic Ag. This led to the formation of Ag agglomerates ideal for SERS applications as noted by the detection of nanomolar concentrations of MB and fungicide thiram. The enhancement factor for MB and thiram probes were 9.3 x 10^4 and 1.5 x 10^5, respectively. We will further push the limit of detection of these platforms and incursion into the ability of these graphene stacking configurations as sensing platforms toward small concentrations of analytes.

ASOCIATED CONTENT

Supporting Information Available

Raman spectra of as-grown graphene with different stacking configurations along with Raman spectra evaluating molecular doping. Scanning electron microscopy (SEM) images of Au nanoparticles at the heterojunction. UV-vis diffuse reflectance spectra for the platforms. Raman spectra of the platforms comparing SERS performance. Raman spectra and SEM images of the platforms corresponding to Ni foam and as-grown graphene after Ag galvanic exchange for evaluating SERS activity of these platforms. This material is available free of charge via the Internet at http://pubs.acs.org.

AUTHOR INFORMATION

Corresponding Author

* Francisco J. Ibañez e-mail: fjiban@inifta.unlp.edu.ar.

Phone: +54 (221) 425 7430/7296-Ext: 179. Fax: +54 (221) 425 4642

Notes

The authors declare no competing financial interest.

ACKNOWLEDGEMENTS.

We gratefully acknowledge financial support from CONICET (PIP-0917) and YPF-TECNOLOGÍA (Y-TEC). We also acknowledge Dr. Mauro Cuevas (University of Buenos Aires, Argentina) for fruitful discussions concerning graphene grown on curved areas and Dr. Pablo S. Fernández (IQ-Unicam, Campinas, Brazil) for providing one of the samples used in this work. We are grateful to Alejandra Floridia (Y-TEC) for SEM images and Dr. Marcos E. Coustet (Y-TEC) for his help during the elaboration of this work. Mercedes Messina acknowledges Dr. M. Celeste Dalfovo (INIFTA) for helping out with graphene synthesis on Ni foam.

References

(1) Chen, N.; Pan, Q. Versatile Fabrication of Ultralight Magnetic Foams and Application for Oil–Water Separation. *ACS Nano* **2013**, *7* (8), 6875–6883.

(2) Cao, X.; Shi, Y.; Shi, W.; Lu, G.; Huang, X.; Yan, Q.; Zhang, Q.; Zhang, H. Preparation of Novel 3D Graphene Networks for Supercapacitor Applications. *Small* **2011**, *7* (22), 3163–3168.

(3) Li, N.; Chen, Z.; Ren, W.; Li, F.; Cheng, H.-M. Flexible Graphene-Based Lithium Ion Batteries with Ultrafast Charge and Discharge Rates. *Proc. Natl. Acad. Sci.* **2012**, *109* (43), 17360–17365.

(4) Lee, S.; Hahm, M. G.; Vajtai, R.; Hashim, D. P.; Thurakitseree, T.; Chipara, A. C.; Ajayan, P. M.; Hafner, J. H. Utilizing 3D SERS Active Volumes in Aligned Carbon Nanotube Scaffold Substrates. *Adv. Mater.* **2012**, *24* (38), 5261–5266.

(5) Ferrari, A. C.; Meyer, J. C.; Scardaci, V.; Casiraghi, C.; Lazzeri, M.; Mauri, F.; Piscanec, S.; Jiang, D.; Novoselov, K. S.; Roth, S.; et al. Raman Spectrum of Graphene and Graphene Layers. *Phys. Rev. Lett.* **2006**, *97* (18), 187401.

(6) Malard, L. M.; Pimenta, M. A.; Dresselhaus, G.; Dresselhaus, M. S. Raman Spectroscopy in Graphene. *Phys. Rep.* **2009**, *473* (5), 51–87.

(7) Ling, X.; Xie, L.; Fang, Y.; Xu, H.; Zhang, H.; Kong, J.; Dresselhaus, M. S.; Zhang, J.; Liu, Z. Can Graphene Be Used as a Substrate for Raman Enhancement? *Nano Lett.* **2010**, *10* (2), 553–561.

(8) Xu, W.; Mao, N.; Zhang, J. Graphene: A Platform for Surface-Enhanced Raman Spectroscopy. *Small Weinh. Bergstr. Ger.* **2013**, *9* (8), 1206–1224.

(9) Lin, W.-H.; Lu, Y.-H.; Hsu, Y.-J. Au Nanoplates as Robust, Recyclable SERS Substrates for Ultrasensitive Chemical Sensing. *J. Colloid Interface Sci.* **2014**, *418*, 87–94.

(10) Qiu, L.; Wang, W.; Zhang, A.; Zhang, N.; Lemma, T.; Ge, H.; Toppari, J. J.; Hytönen, V. P.; Wang, J. Core–Shell Nanorod Columnar Array Combined with Gold Nanoplate–Nanosphere Assemblies Enable Powerful In Situ SERS Detection of Bacteria. *ACS Appl. Mater. Interfaces* **2016**, *8* (37), 24394–24403.

(11) Zhang, J.; He, L.; Chen, P.; Tian, C.; Wang, J.; Liu, B.; Jiang, C.; Zhang, Z. A Silica-Based SERS Chip for Rapid and Ultrasensitive Detection of Fluoride Ions Triggered by a Cyclic Boronate Ester Cleavage Reaction. *Nanoscale* **2017**, *9* (4), 1599–1606.

(12) Dalfovo, M. C.; Lacconi, G. I.; Moreno, M.; Yappert, M. C.; Sumanasekera, G. U.; Salvarezza, R. C.; Ibañez, F. J. Synergy between Graphene and Au Nanoparticles (Heterojunction) towards Quenching, Improving Raman Signal, and UV Light Sensing. *ACS Appl. Mater. Interfaces* **2014**, *6* (9), 6384–6391.

(13) Pérez, L. A.; Dalfovo, M. C.; Troiani, H.; Soldati, A. L.; Lacconi, G. I.; Ibañez, F. J. CVD Graphene Transferred with Au Nanoparticles: An Ideal Platform for TERS and SERS on a Single Triangular Nanoplate. *J. Phys. Chem. C* **2016**, *120* (15), 8315–8322.

(14) Chen, Z.; Berciaud, S.; Nuckolls, C.; Heinz, T. F.; Brus, L. E. Energy Transfer from Individual Semiconductor Nanocrystals to Graphene. *ACS Nano* **2010**, *4* (5), 2964–2968.

(15) Wilcoxon, J. P.; Martin, J. E.; Parsapour, F.; Wiedenman, B.; Kelley, D. F. Photoluminescence from Nanosize Gold Clusters. *J. Chem. Phys.* **1998**, *108* (21), 9137–9143.

(16) Dahal, A.; Batzill, M. Graphene–nickel Interfaces: A Review. *Nanoscale* **2014**, *6* (5), 2548–2562.

(17) Sung, C.-M.; Tai, M.-F. Reactivities of Transition Metals with Carbon: Implications to the Mechanism of Diamond Synthesis under High Pressure. *Int. J. Refract. Met. Hard Mater.* **1997**, *15* (4), 237–256.

(18) Li, X.; Cai, W.; Colombo, L.; Ruoff, R. S. Evolution of Graphene Growth on Ni and Cu by Carbon Isotope Labeling. *Nano Lett.* **2009**, *9* (12), 4268–4272.

(19) Seah, C.-M.; Chai, S.-P.; Mohamed, A. R. Mechanisms of Graphene Growth by Chemical Vapour Deposition on Transition Metals. *Carbon* **2014**, *70* (Supplement C), 1–21.

(20) Takahashi, K.; Yamada, K.; Kato, H.; Hibino, H.; Homma, Y. In Situ Scanning Electron Microscopy of Graphene Growth on Polycrystalline Ni Substrate. *Surf. Sci.* **2012**, *606* (7), 728–732.

(21) Allard, A.; Wirtz, L. Graphene on Metallic Substrates: Suppression of the Kohn Anomalies in the Phonon Dispersion. *Nano Lett.* **2010**, *10* (11), 4335–4340.

(22) Lu, C.-C.; Lin, Y.-C.; Liu, Z.; Yeh, C.-H.; Suenaga, K.; Chiu, P.-W. Twisting Bilayer Graphene Superlattices. *ACS Nano* **2013**, *7* (3), 2587–2594.

(23) Carozo, V.; Almeida, C. M.; Ferreira, E. H. M.; Cançado, L. G.; Achete, C. A.; Jorio, A. Raman Signature of Graphene Superlattices. *Nano Lett.* **2011**, *11* (11), 4527–4534.

(24) Kim, K.; Coh, S.; Tan, L. Z.; Regan, W.; Yuk, J. M.; Chatterjee, E.; Crommie, M. F.; Cohen, M. L.; Louie, S. G.; Zettl, A. Raman Spectroscopy Study of Rotated Double-Layer Graphene: Misorientation-Angle Dependence of Electronic Structure. *Phys. Rev. Lett.* **2012**, *108* (24), 246103.

(25) Ek Weis, J.; Costa, S. D.; Frank, O.; Bastl, Z.; Kalbac, M. Fluorination of Isotopically Labeled Turbostratic and Bernal Stacked Bilayer Graphene. *Chem. – Eur. J.* **2015**, *21* (3), 1081–1087.

(26) Ek Weis, J.; Costa, S.; Frank, O.; Fridrichová, M.; Vlčková, B.; Vejpravova, J.; Kalbac, M. SERS of Isotopically Labeled 12C/13C Graphene Bilayer–Gold Nanostructured Film Hybrids: Graphene Layer as Spacer and SERS Probe. *J. Phys. Chem. C* **2017**, *121* (21), 11680–11686.

(27) Latil, S.; Meunier, V.; Henrard, L. Massless Fermions in Multilayer Graphitic Systems with Misoriented Layers: Ab Initio Calculations and Experimental Fingerprints. *Phys Rev B* **2007**, *76*.

(28) Cao, Y.; Fatemi, V.; Fang, S.; Watanabe, K.; Taniguchi, T.; Kaxiras, E.; Jarillo-Herrero, P. Unconventional Superconductivity in Magic-Angle Graphene Superlattices. *Nature* **2018**.

(29) Lee, J.; Novoselov, K. S.; Shin, H. S. Interaction between Metal and Graphene: Dependence on the Layer Number of Graphene. *ACS Nano* **2011**, *5* (1), 608–612.

(30) Voggu, R.; Das, B.; Rout, C. S.; Rao, C. N. R. Effects of Charge Transfer Interaction of Graphene with Electron Donor and Acceptor Molecules Examined Using Raman Spectroscopy and Cognate Techniques. *J. Phys. Condens. Matter* **2008**, *20* (47), 472204.

(31) Dong, X.; Fu, D.; Fang, W.; Shi, Y.; Chen, P.; Li, L.-J. Doping Single-Layer Graphene with Aromatic Molecules. *Small* **2009**, *5* (12), 1422–1426.

(32) Singh, A. K.; Iqbal, M. W.; Singh, V. K.; Iqbal, M. Z.; Lee, J. H.; Chun, S.-H.; Shin, K.; Eom, J. Molecular N-Doping of Chemical Vapor Deposition Grown Graphene. *J. Mater. Chem.* **2012**, *22* (30), 15168–15174.

(33) Alam, R.; Lightcap, I. V.; Karwacki, C. J.; Kamat, P. V. Sense and Shoot: Simultaneous Detection and Degradation of Low-Level Contaminants Using Graphene-Based Smart Material Assembly. *ACS Nano* **2014**, *8* (7), 7272–7278.

(34) Zhao, H.; Jin, J.; Tian, W.; Li, R.; Yu, Z.; Song, W.; Cong, Q.; Zhao, B.; Ozaki, Y. Three-Dimensional Superhydrophobic Surface-Enhanced Raman Spectroscopy Substrate for Sensitive Detection of Pollutants in Real Environments. *J. Mater. Chem. A* **2015**, *3* (8), 4330–4337.

(35) Verlato, E.; He, W.; Amrane, A.; Barison, S.; Floner, D.; Fourcade, F.; Geneste, F.; Musiani, M.; Seraglia, R. Preparation of Silver-Modified Nickel Foams by Galvanic Displacement and Their Use as Cathodes for the Reductive Dechlorination of Herbicides. *ChemElectroChem* **2016**, *3* (12), 2084–2092.

(36) Gutés, A.; Maboudian, R.; Carraro, C. Gold-Coated Silver Dendrites as SERS Substrates with an Improved Lifetime. *Langmuir* **2012**, *28* (51), 17846–17850.

(37) Gutés, A.; Carraro, C.; Maboudian, R. Silver Dendrites from Galvanic Displacement on Commercial Aluminum Foil As an Effective SERS Substrate. *J. Am. Chem. Soc.* **2010**, *132* (5), 1476–1477.

(38) Prasai, D.; Tuberquia, J. C.; Harl, R. R.; Jennings, G. K.; Bolotin, K. I. Graphene: Corrosion-Inhibiting Coating. *ACS Nano* **2012**, *6* (2), 1102–1108.

(39) Usman, M.; Pan, L.; Sohail, A.; Mahmood, Z.; Cui, R. Fabrication of 3D Vertically Aligned Silver Nanoplates on Nickel Foam-Graphene Substrate by a Novel Electrodeposition with Sonication for Efficient Supercapacitors. *Chem. Eng. J.* **2017**, *311*, 359–366.

(40) United States. Environmental Protection Agency: Thiram. REREGISTRATION ELIGIBILITY DECISION. List A CASE 0122. 2004.

(41) Chen, Z.; Ren, W.; Gao, L.; Liu, B.; Pei, S.; Cheng, H.-M. Three-Dimensional Flexible and Conductive Interconnected Graphene Networks Grown by Chemical Vapour Deposition. *Nat. Mater.* **2011**, *10* (6), 424–428.

(42) Fink, J.; Kiely, C. J.; Bethell, D.; Schiffrin, D. J. Self-Organization of Nanosized Gold Particles. *Chem. Mater.* **1998**, *10* (3), 922–926.

(43) Dalfovo, M. C.; Salvarezza, R. C.; Ibañez, F. J. Improved Vapor Selectivity and Stability of Localized Surface Plasmon Resonance with a Surfactant-Coated Au Nanoparticles Film. *Anal. Chem.* **2012**, *84* (11), 4886–4892.

(44) Yoon, T.; Kim, J.-H.; Choi, J. H.; Jung, D. Y.; Park, I.-J.; Choi, S.-Y.; Cho, N. S.; Lee, J.-I.; Kwon, Y.-D.; Cho, S.; et al. Healing Graphene Defects Using Selective Electrochemical Deposition: Toward Flexible and Stretchable Devices. *ACS Nano* **2016**, *10* (1), 1539–1545.

(45) Ambrosi, A.; Bonanni, A.; Sofer, Z.; Pumera, M. Large-Scale Quantification of CVD Graphene Surface Coverage. *Nanoscale* **2013**, *5* (6), 2379–2387.

(46) Kozlova, J.; Niilisk, A.; Alles, H.; Sammelselg, V. Discontinuity and Misorientation of Graphene Grown on Nickel Foil: Effect of the Substrate Crystallographic Orientation. *Carbon* **2015**, *94* (Supplement C), 160–173.

(47) Niilisk, A.; Kozlova, J.; Alles, H.; Aarik, J.; Sammelselg, V. Raman Characterization of Stacking in Multi-Layer Graphene Grown on Ni. *Carbon* **2016**, *98*, 658–665.

(48) Yu, Y.; Li, Z.; Wang, W.; Guo, X.; Jiang, J.; Nan, H.; Ni, Z. Investigation of Multilayer Domains in Large-Scale CVD Monolayer Graphene by Optical Imaging. *J. Semicond.* **2017**, *38* (3), 033003.

(49) Wang, Y.; Ni, Z.; Liu, L.; Liu, Y.; Cong, C.; Yu, T.; Wang, X.; Shen, D.; Shen, Z. Stacking-Dependent Optical Conductivity of Bilayer Graphene. *ACS Nano* **2010**, *4* (7), 4074–4080.

(50) Pirruccio, G.; Martín Moreno, L.; Lozano, G.; Gómez Rivas, J. Coherent and Broadband Enhanced Optical Absorption in Graphene. *ACS Nano* **2013**, *7* (6), 4810–4817.

(51) Cong, C.; Yu, T.; Saito, R.; Dresselhaus, G. F.; Dresselhaus, M. S. Second-Order Overtone and Combination Raman Modes of Graphene Layers in the Range of 1690−2150 Cm−1. *ACS Nano* **2011**, *5* (3), 1600–1605.

(52) Rao, R.; Podila, R.; Tsuchikawa, R.; Katoch, J.; Tishler, D.; Rao, A. M.; Ishigami, M. Effects of Layer Stacking on the Combination Raman Modes in Graphene. *ACS Nano* **2011**, *5* (3), 1594–1599.

(53) He, R.; Chung, T.-F.; Delaney, C.; Keiser, C.; Jauregui, L. A.; Shand, P. M.; Chancey, C. C.; Wang, Y.; Bao, J.; Chen, Y. P. Observation of Low Energy Raman Modes in Twisted Bilayer Graphene. *Nano Lett.* **2013**, *13* (8), 3594–3601.

(54) Gupta, A. K.; Nisoli, C.; Lammert, P. E.; Crespi, V. H.; Eklund, P. C. Curvature-Induced D-Band Raman Scattering in Folded Graphene. *J. Phys. Condens. Matter Inst. Phys. J.* **2010**, *22* (33), 334205.

(55) Barros, E. B.; Demir, N. S.; Souza Filho, A. G.; Mendes Filho, J.; Jorio, A.; Dresselhaus, G.; Dresselhaus, M. S. Raman Spectroscopy of Graphitic Foams. *Phys. Rev. B* **2005**, *71* (16), 165422.

(56) Durhuus, D.; Larsen, M. V.; Andryieuski, A.; Malureanu, R.; Pizzocchero, F.; Bøggild, P.; Lavrinenko, A. V. Selective Electroless Silver Deposition on Graphene Edges. *J. Electrochem. Soc.* **2015**, *162* (6), D213–D217.

(57) Li, Z.; Zhang, P.; Wang, K.; Xu, Z.; Wei, J.; Fan, L.; Wu, D.; Zhu, H. Graphene Buffered Galvanic Synthesis of Graphene–metal Hybrids. *J. Mater. Chem.* **2011**, *21* (35), 13241–13246.

(58) Matz, D. L.; Sojoudi, H.; Graham, S.; Pemberton, J. E. Signature Vibrational Bands for Defects in CVD Single-Layer Graphene by Surface-Enhanced Raman Spectroscopy. *J. Phys. Chem. Lett.* **2015**, *6* (6), 964–969.

(59) Zhou, H.; Qiu, C.; Yu, F.; Yang, H.; Chen, M.; Hu, L.; Sun, L. Thickness-Dependent Morphologies and Surface-Enhanced Raman Scattering of Ag Deposited on n-Layer Graphenes. *J. Phys. Chem. C* **2011**, *115* (23), 11348–11354.

(60) Giovannetti, G.; Khomyakov, P. A.; Brocks, G.; Karpan, V. M.; van den Brink, J.; Kelly, P. J. Doping Graphene with Metal Contacts. *Phys. Rev. Lett.* **2008**, *101* (2), 026803.

(61) Tripathi, A.; Emmons, E. D.; Fountain, A. W.; Guicheteau, J. A.; Moskovits, M.; Christesen, S. D. Critical Role of Adsorption Equilibria on the Determination of Surface-Enhanced Raman Enhancement. *ACS Nano* **2015**, *9* (1), 584–593.

(62) Le Ru, E. C.; Blackie, E.; Meyer, M.; Etchegoin, P. G. Surface Enhanced Raman Scattering Enhancement Factors: A Comprehensive Study. *J. Phys. Chem. C* **2007**, *111* (37), 13794–13803.

(63) Xu, W.; Ling, X.; Xiao, J.; Dresselhaus, M. S.; Kong, J.; Xu, H.; Liu, Z.; Zhang, J. Surface Enhanced Raman Spectroscopy on a Flat Graphene Surface. *Proc. Natl. Acad. Sci.* **2012**, *109* (24), 9281–9286.

Figures and Captions

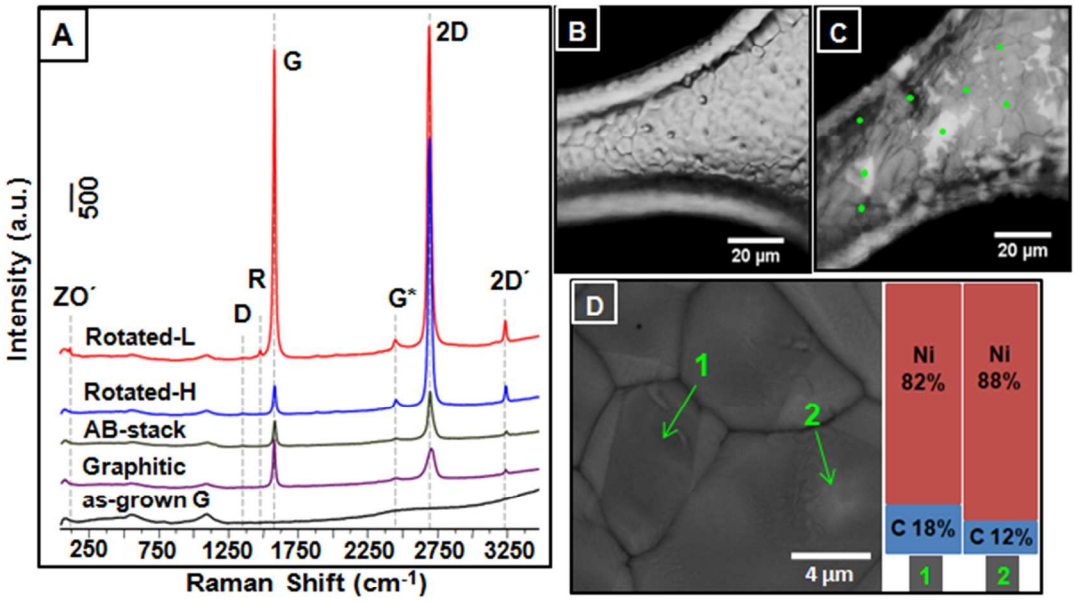

Figure 1. Representative Raman spectra acquired at five different areas of the same Ni foam sample after graphene growth (A). Optical images before (B) and after (C) graphene growth. Green dots represent the different regions evaluated for the analysis. SEM image taken from the same sample after graphene growth (D). Green arrows indicate two regions with different carbon content showing that darker spots (labeled "1") contains more carbon than the brighter spot labeled "2" as indicated in the bar chart on the right of the image.

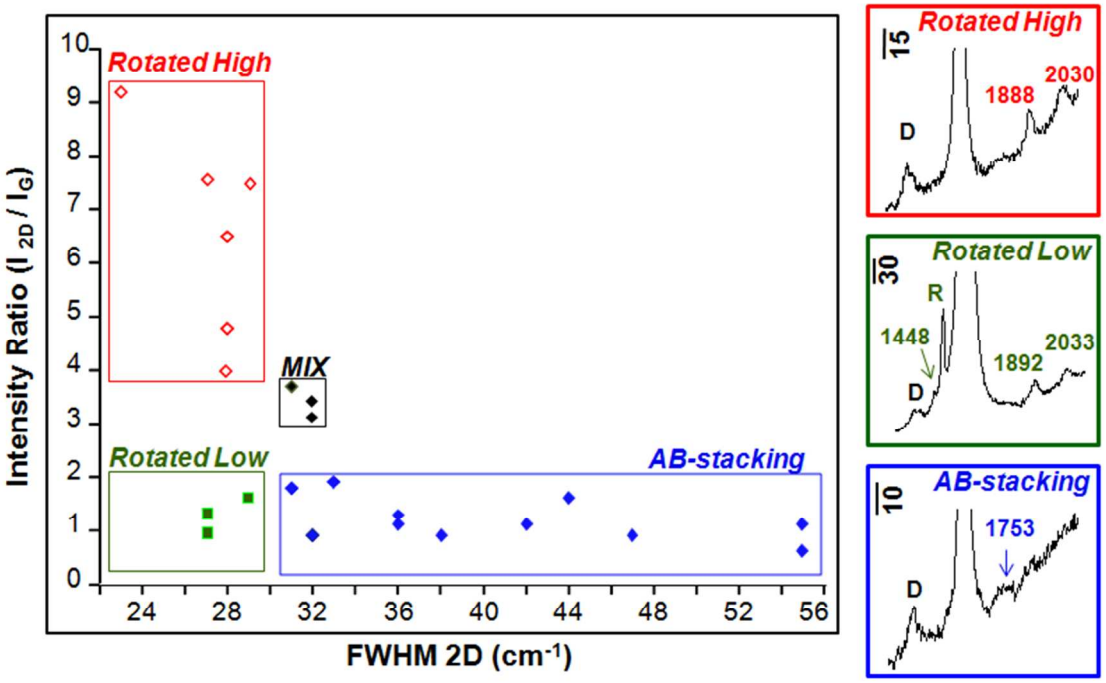

Figure 2. Intensity ratio (I_{2D}/I_G) vs. full-width half-maximum (fwhm) plot of the 2D band taken from 23 different areas of as-grown graphene along with representative Raman spectra (shown aside the plot) corresponding to the three different stacking configurations.

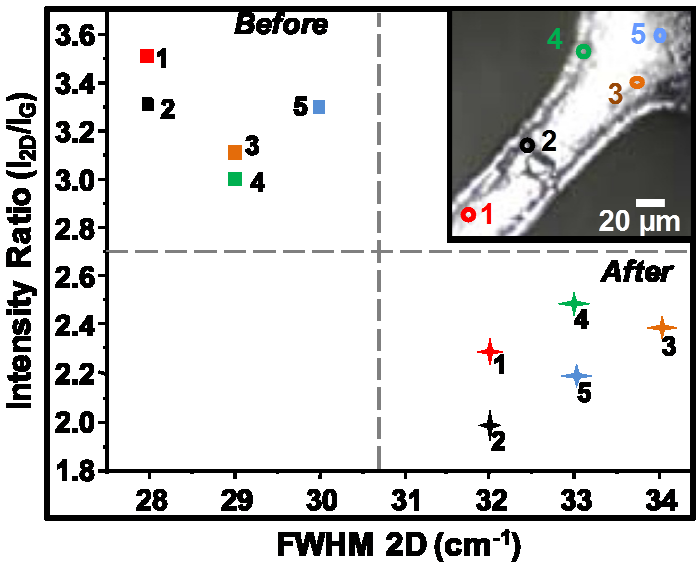

Figure 3. Intensity ratio (I_{2D}/I_G) vs. full-width half-maximum (fwhm) plot of the 2D band measured from 5 different areas of as-grown sample (rotated-H) before and after the addition of [MB] = 1.0 x 10^{-6} M. The optical image (inset of the figure) shows the exact Raman spots evaluated for the analysis.

Table 1. Intensity ratio, 2D FWHM, and Raman Shift from all the spots shown in Fig. 3 acquired before and after addition of MB. The table also shows the Avg. Raman shift of 2D band and Avg. intensity ratio (I2D/IG) pointing out the doping effect of the analyte molecule in graphene bands.

Spot	Sample	I_{2D}/I_G	2D FWHM (cm^{-1})	2D Raman Shift (cm^{-1})
1	Before	3.5	28	2704
	After	2.3	32	2701
2	Before	3.3	28	2704
	After	2.0	32	2702
3	Before	3.1	29	2701
	After	2.4	34	2699
4	Before	3.0	29	2700
	After	2.5	33	2697
5	Before	3.3	30	2702
	After	2.2	33	2700
	Avg. 2D Raman Shift (cm^{-1})		Avg. Intensity Ratio (I_{2D}/I_G)	
before	2702 ± 2		3.2 ± 0.2	
after	2700 ± 2		2.3 ± 0.2	

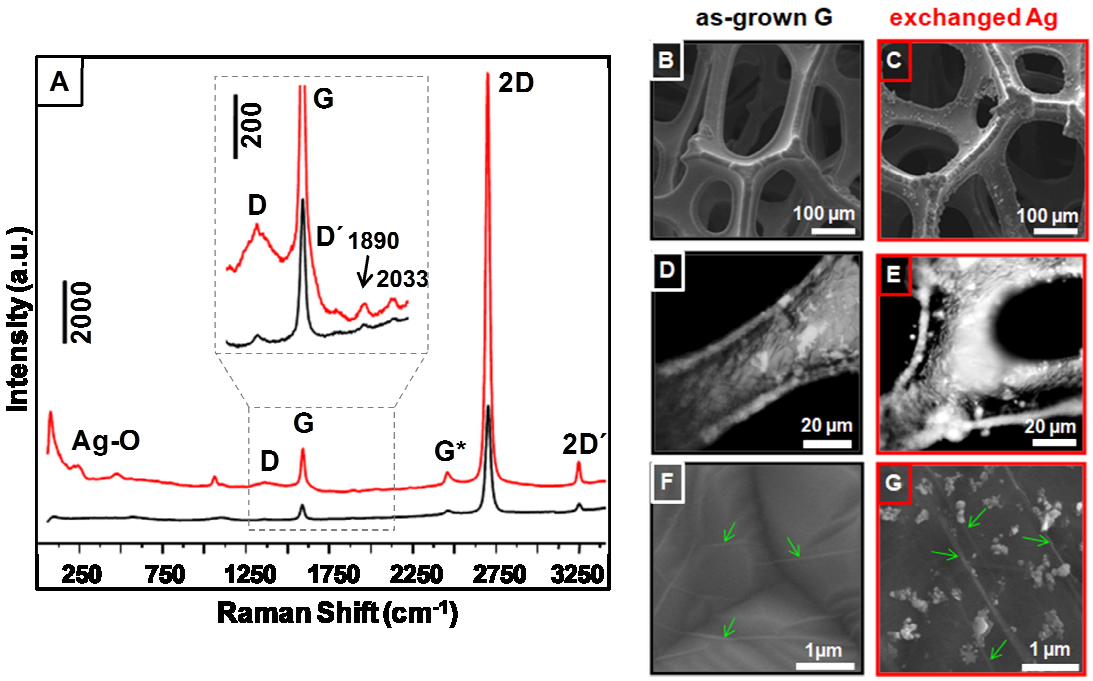

Figure 4. Selected Raman spectra for the as-grown sample (rotated-High stacking) before and after Ag galvanic exchange (red spectrum located above)(A). The inset corresponds to a zoom-in exhibiting “in-plane modes” and new bands aroused from Ag interaction. Optical (D and E) and SEM (B, C, F, and G) images of as-grown sample before and after 5 min Ag exchange.

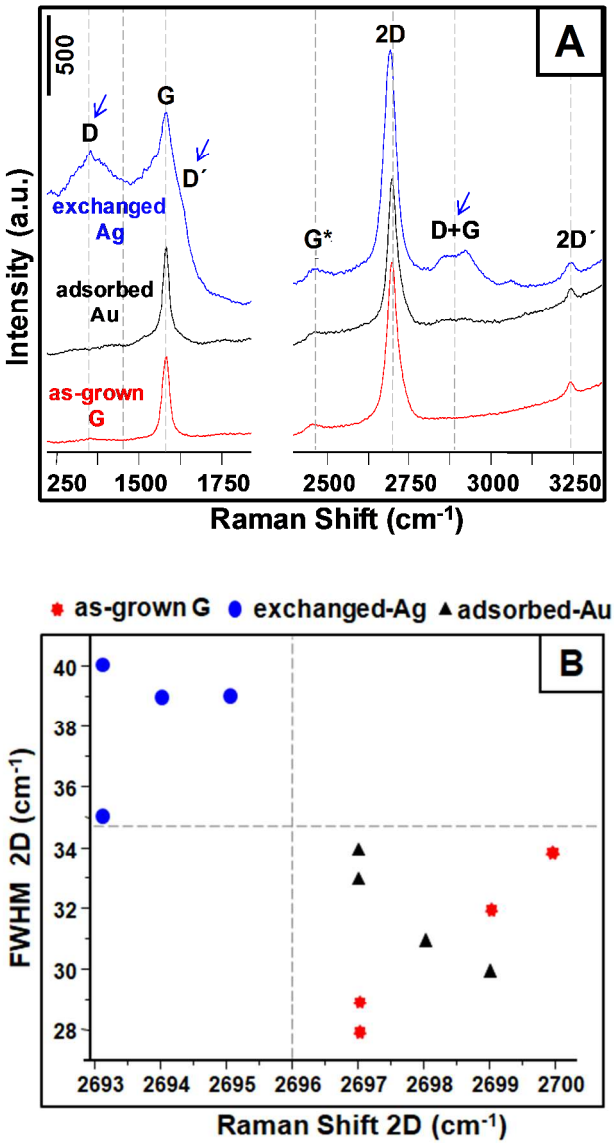

Figure 5. Representative Raman spectra of as-grown graphene, Au NPs adsorbed, and Ag galvanic exchanged (A). Plot of fwhm vs. Raman shift of the 2D band taken from the three samples as indicated (B).

Table 2. Average FWHM and Raman Shift of 2D band measured for as-grown graphene, exchange Ag, and adsorbed Au samples.

	Average 2D FWHM (cm^{-1})	Average Raman Shift (cm^{-1})
as-grown G	31 ± 3	2698 ± 2
exchanged Ag	38 ± 2	2694 ± 1
adsorbed Au	32 ± 2	2698 ± 1

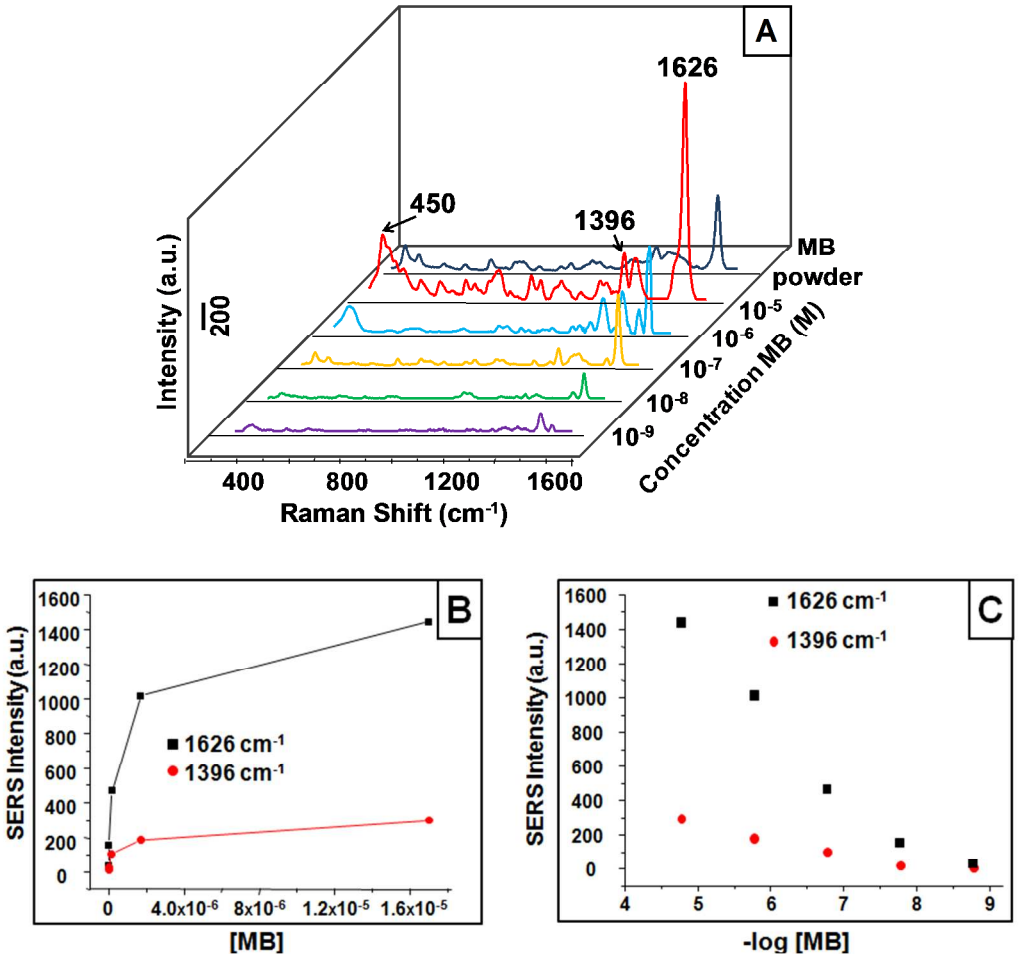

Figure 6. Representative Raman spectra for Ag exchanged platform measured at various concentrations of MB ranging from 10^{-5} to 10^{-9} M compared with Raman signal from the solid analyte (A). Plot shows SERS intensity versus concentration of MB (B) and SERS intensity versus logarithm of MB concentration (C) for the peaks located at 1396 cm^{-1} and 1626 cm^{-1}.

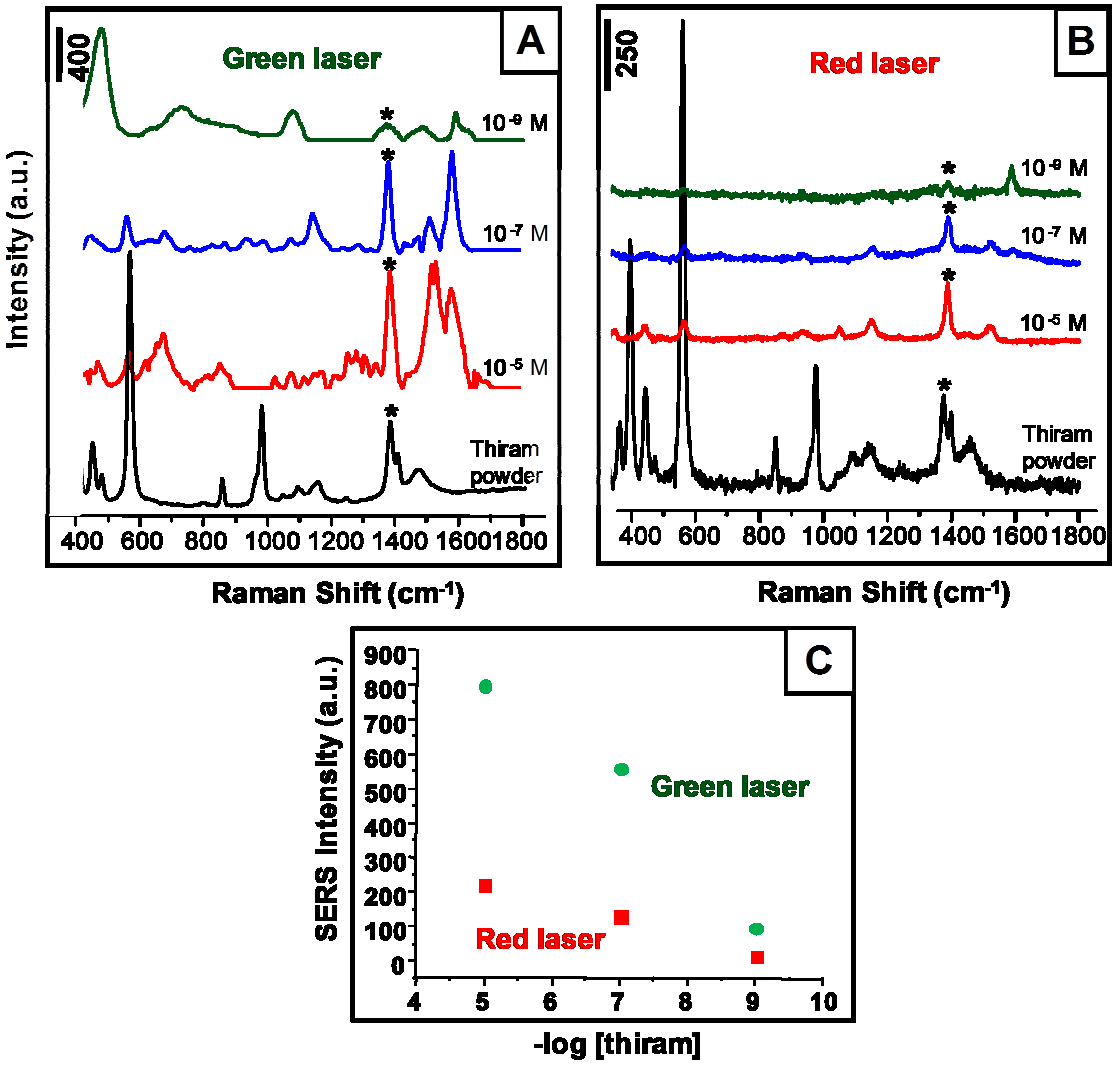

Figure 7. Representative Raman spectra for the platform Ag exchanged for three specific concentrations of thiram (10^{-5}, 10^{-7}, and 10^{-9} M) compared with Raman signal from the solid analyte. Two different excitation wavelength were compared, green (A) and red (B). Plot shows SERS intensity vs. logarithmic concentration of thiram for the peak located at 1386 cm^{-1} for green and red laser (C).

TOC

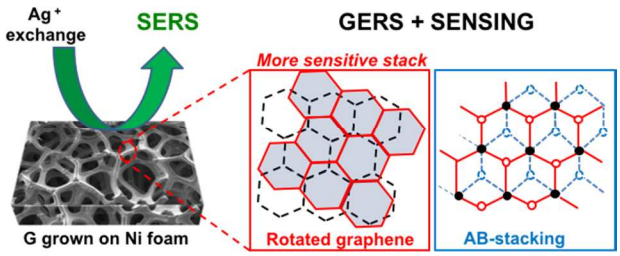
Ag+ exchange
SERS
GERS + SENSING
More sensitive stack
G grown on Ni foam
Rotated graphene
AB-stacking